Contents lists available at ScienceDirect

Journal of Electroanalytical Chemistry

journal homepage: http://ees.elsevier.com

Hybrid nanomaterial/catalase-modified electrode for hydrogen peroxide sensing

Dayana Soto [a], Manuela Alzate [b], Jaime Gallego [b], Jahir Orozco [a,*]

[a] Max Planck Tandem Group in Nanobioengieneering, University of Antioquia, Complejo Ruta N, Calle 67 N° 52-20, Medellín, Colombia
[b] Química de Recursos Energéticos y Medio Ambiente, Instituto de Química, University of Antioquia, Calle 70 N° 52-21, Medellín, Colombia

ARTICLE INFO

Keywords
Hybrid nanomaterial
Graphene
Iron nanoparticles
Catalase
Direct electrochemistry

ABSTRACT

Conjugation of biomolecules with hybrid nanomaterials offer opportunities in the assembly of (bio)sensors of improved electrochemical performance. This work reports on developing a novel catalase-functionalized hybrid nanomaterial for the detection of hydrogen peroxide (H_2O_2). The rationally assembled (bio)sensor consists of iron nanoparticles coated with graphene's layers supported on multi-walled carbon nanotubes (Fe@G-MWCNTs), deposited at a screen-printed carbon electrode surface and functionalized with catalase. Transmission electron microscopy, X-ray diffraction-, X-ray photoelectron-, thermogravimetric-analysis were used to characterize the physicochemical properties of the hybrid nanomaterial and better understand its electrochemical behavior. The (bio)sensor response was linear from 0.1 to 7 mM, with a sensitivity of 0.059 μA/(μM.cm^2), a limit of detection of 28.2 μM, a Michaelis-Menten constant of 17.9 mM, and high reproducibility. The graphene flakes acted as a protective layer that prevented the loss of the Fe nanoparticles activity, thus improving the long-term stability of the (bio)sensor.

1. Introduction

Electrochemical sensing platforms and functional interfaces exploit hybrid nanomaterials to improve performance. Hybrid materials combine organic and inorganic building blocks that working together generate a synergic effect of improved performance concerning the individual components acting alone [1,2]. Multi-walled carbon nanotubes (MWCNTs) are hollow cylinders of multiple graphite layers superimposed and rolled, composed of conjugated sp^2-carbon atoms arranged into a planner 2D honeycomb lattice [1]. MWCNTs have attracted particular interest as supporting nanomaterial in functional interfaces due to their unique electronic, structural, mechanical and catalytic properties; and their amenability for functionalization [4–6]. The electronic properties of the MWCNTs are governed mainly by the outermost layer that is also chemically very active. However, their trend to aggregation and the non-uniform surface defects generated during the synthesis process hinder the electron transfer and limit their application in (bio)sensor devices.

Different strategies have been assessed to overcome such limitations, including modification of MWCNTs with metallic nanoparticles [4,7], which have been widely used in biosensing because of their bioactivity, biocompatibility, and electro-conductive properties [8,9]. Nanomaterials based on iron nanoparticles offer additional advantages over nanoparticles from other metals (e.g., Au, Pt, Pd) that are related to its availability, low production cost and magnetic properties [10–12]. However, changes in the medium conditions, such as pH and temperature, may generate variations in their oxidation state that may affect their electrical properties and limit their use in electrochemical sensing devices [13,14].

Graphene is a single atomic layer of graphite carbon made by sp^2 carbon atoms arranged in a hexagonal lattice, which sheets have even a 2-fold surface area than MWCNTs. Moreover, graphene has high mechanical strength, low density, intrinsic flexibility and very high electron mobility due to a free π electron for each carbon atom available for electronic conduction [15]. The use of graphene as a protective coating for metallic nanostructures has been of great interest because of graphene's ability to isolate the metallic metal surface, inhibiting its corrosion and allowing the charge transfer through the metal-graphene interface [16,17]. Metals coated with graphene sheets generate core-shell-like type structures with high chemical stability, but with some hindering of their catalytic activity [18].

Catalase (Cat) is an oxidoreductase that exists as a tetramer of four identical subunits (220–350 kD), present in the peroxisomes of nearly all aerobic cells to protect them from the toxic effects of H_2O_2. Each subunit contains a heme prosthetic group at the catalytic center that consists of a protoporphyrin ring and a central Fe atom in the ferric —Fe (III)- state [19,20]. Direct electron exchange of enzymes and electrodes not only gives an insight into their mechanistic processes and catalytic activity but simplify third-generation (bio)sensors by avoiding the requirements of chemical mediators [21,22]. We have already demonstrated the stability, conductive properties and catalytic activity of the Fe@G-MWCNTs hybrid nanomaterial [23]. However, this is the first report exploiting its potential as a support for the immobilization of bioreceptors and (bio)sensor development.

* Corresponding author.
E-mail address: grupotandem.nanobioe@udea.edu.co (J. Orozco)

https://doi.org/10.1016/j.jelechem.2020.114826
Received 14 July 2020; Received in revised form 14 October 2020; Accepted 2 November 2020
Available online xxx
1572-6657/

Herein, we describe an electrochemical (bio)-sensor's development based on a catalase-functionalized hybrid nanomaterial for sensing H_2O_2. Catalase was immobilized on the surface of a rationally assembled hybrid nanomaterial based on MWCNTs, with Fe nanoparticles grown at the nanotubes' surface and coated with few graphene layers (Cat-Fe@G-MWCNTs). Unlike common hybrid nanomaterials assembled by a random mix of their components, we report rationally but naturally disposed nanomaterials assembled one-by-one and systematically compared their electrochemical performance. A diffusion-controlled redox process at faster electron-transfer at the bare hybrid and a higher density of Cat immobilized at its surface accounted for the enhanced electrocatalytic performance of the resultant H_2O_2 (bio)sensor, with respect to the concomitant counterparts. The graphene flakes acted as a protective layer that prevented the loss of the Fe nanoparticles catalytic activity, thus improving the (bio)sensor's long-term stability. This is the first enzymatic (bio)sensor with the hybrid nanomaterial, but it offers opportunities for the development of a myriad of specific and highly sensitive Fe@G-MWCNTs hybrid nanomaterial-based (bio)sensors.

2. Experimental

2.1. Reagents

Catalase solution (E.C. 1.11.1.6) from bovine liver (10.000–40.000 units/mg protein), potassium ferricyanide (III) ($K_3[Fe(CN)_6]$), potassium hexacyanoferrate (II) trihydrate ($K_4[Fe(CN)_6].3H_2O$) and hydrogen peroxide aqueous solution (H_2O_2) of 30% volumetric fraction were purchased from Merck Millipore (Darmstadt, Germany). Dipotassium hydrogen phosphate (K_2HPO_4), disodium hydrogen phosphate (Na_2HPO_4) and potassium nitrate (KNO_3) were acquired from PanReac AppliChem (Darmstadt, Germany). Potassium dihydrogen phosphate (KH_2PO_4), potassium chloride (KCl) and sodium chloride (NaCl) were obtained from J.T.Baker® (Xalostoc, Mexico). Sulphuric acid (H_2SO_4) was purchased from Honeywell FlukaTM (Seelve, Germany). N-(3-dimethylaminopropyl)-N′-ethylcarbodiimide hydrochloride (EDC), N-hydroxysuccinimide (NHS), 2-(N-morpholino) ethanesulfonic acid sodium salt (MES) were purchased from Sigma-Aldrich (Saint Louis, MO, USA). The commercial samples were purchased from a local pharmacy in Medellín, Colombia (6°15′06.6"N 75°33′48.9"W). They consist of an antiseptic solution and Dioxogen samples with a nominal composition of H_2O_2 of 4 and 3.6% H_2O_2, respectively, from JgB®. A creamy lotion of 9.0% H_2O_2 nominal composition was from IGORA Schwarzkopf. Each sample was diluted in PBS 1 × (pH 7.2)/N_2 saturated solution to a concentration of 3.0 mM H_2O_2. All reagents and commercial samples were used without purification and the solutions were prepared using deionized water.

2.2. Apparatus

Morphology, structural and compositional analysis of the hybrid nanomaterials were characterized by high-resolution transmission electron microscopy (HR-TEM), thermogravimetric analysis (TGA) and X-ray diffraction (XRD). Particle size and morphological characteristics were measured by HR-TEM by using a JEOL JSM 7100F field-emission gun scanning electron microscope (FEG-SEM) operated at 200 kV as acceleration voltage. TGA experiments were carried out in a TA-Instruments Q500 thermogravimetry analyzer. XRD experiments were conducted in a Panalytical X'PERT PRO MPD diffractometer with CuKα1 = 1.5406 Å, operated at 45 kV and 40 mA. Surface and elemental chemical composition were characterized by X-ray photoelectron spectroscopy (XPS) with a PHOIBOS 150 1D-DLD (SPECS GmbH, Berlin, Germany) photoelectronic X-ray spectrometer (NAP-XPS) analyzer. It used a monochromatic light of Al Kα (1486.7 eV, 13 kV, 100 W) with 100 and 30 eV energy steps for general and high-resolution spectra, which values were 1 and 0.1 eV, respectively. The spectra were analyzed using CasaXPS software.

The electrochemical measurements were performed with a three-electrode cell configuration SPCE, (ref. 150, from DropSens), in a VersaSTAT3 electrochemical workstation with an impedance analyzer. The chips consist of a 4 mm carbon working electrode, a platinum counter electrode, and a silver pseudo-reference electrode, respectively printed on the same strip.

2.3. Preparation and characterization of the Fe@G-MWCNTs hybrid nanomaterial

Fe@G-MWCNTs were prepared according to a previously reported method [23,24], whose experimental details are in the S.I section. The hybrid nanomaterial characterization conditions through HR-TEM, TGA, XRD and XPS are described in the S.I. section.

2.4. Assembly of the enzymatic (bio)sensor

SPCEs were pre-treatment by cyclic voltammetry (CV) in 50 μL of 0.1 M H_2SO_4, scanning the potential between 1.6 and - 0.2 V, followed by CV in a 0.05 M phosphate buffer solution (pH 7.2), scanning between 1.2 and – 1.0 V, at 100 mV/s by 10 consecutive cycles, respectively. Then, 0.5 mg of hybrid nanomaterial were dispersed in 1 mL of PBS 1 × (pH 7.2) solution by a QSONICA Q500 sonicator for 10 s (X2) and 20% amplitude. 6.0 μL of the dispersion was deposited onto the pre-treated SPCE by drop-casting, incubated at 37 °C for 30 min and washed in PBS 1 × (pH 7.2) for removing the not absorbed hybrid nanomaterial. The hybrid nanomaterial modified-electrodes were electrochemically activated in a 0.1 M H_2SO_4 solution by scanning between 1.6 and - 0.2 V (at 100 mV/s), for five cycles. Cat was immobilized on the modified electrodes through the carbodiimide chemistry by adding 6.0 μL of a mixture of 400 mM EDC and 100 mM NHS in 25 mM MES (pH 6.5) and incubation for 30 min. Finally, 6.0 μL of 0.9 mg/mL Cat solution in PBS 1 × (pH 7.2) was dropped on the working electrode, followed by incubation in a wet chamber in a Thermo Scientific MAXQ 4450 shaker at 50 rpm at 37 °C, for 2 h to obtain the Cat/hybrid nanomaterial/SPCE. For comparison, the hybrid nanomaterial/SPCE was also prepared by the same procedure, but without Cat. The enzymatic (bio)sensor assembly and detection mechanism steps are illustrated in the schematic diagram Fig. 1a.

2.5. Electrochemical measurements

CVs were recorded in 50 μL of 1 mM $K_3[Fe(CN)_6]$/PBS 1 × (pH 7.2)/N_2 saturated solution from 0.4 to - 0.2 V at 0.05 V/s scan rate, for five consecutive cycles. Direct communication studies were performed through CV in PBS 1 × (pH 7.2)/N_2 saturated solution by scanning the potential from - 0.1 to - 0.8 V at 0.05 V/s scan rate. Enzymatic activity was studied by CV in a 3.0 mM H_2O_2/PBS 1 × (pH 7.2)/N_2 saturated solution by scanning the potential once from 0.5 to −1.0 V, at 10 mV/s scan rate. Electrochemical impedance spectroscopy (EIS) was conducted at 0.16 V of potential and 0.005 V of amplitude, with a frequency range of 50 kHz – 0.1 Hz. The impedance data were fitted with the software EIS Spectrum Analyzer using the Levenberg-Marquardt algorithm. Chronoamperometry measurements were recorded at a potential of - 0.65 V for 120 s by denoting the amperometry response as the time needed to reach the steady-state current that was estimated to be 30 s. All experiments were recorded using a magnet to confine the nanomaterial at the working electrode from the SPCE.

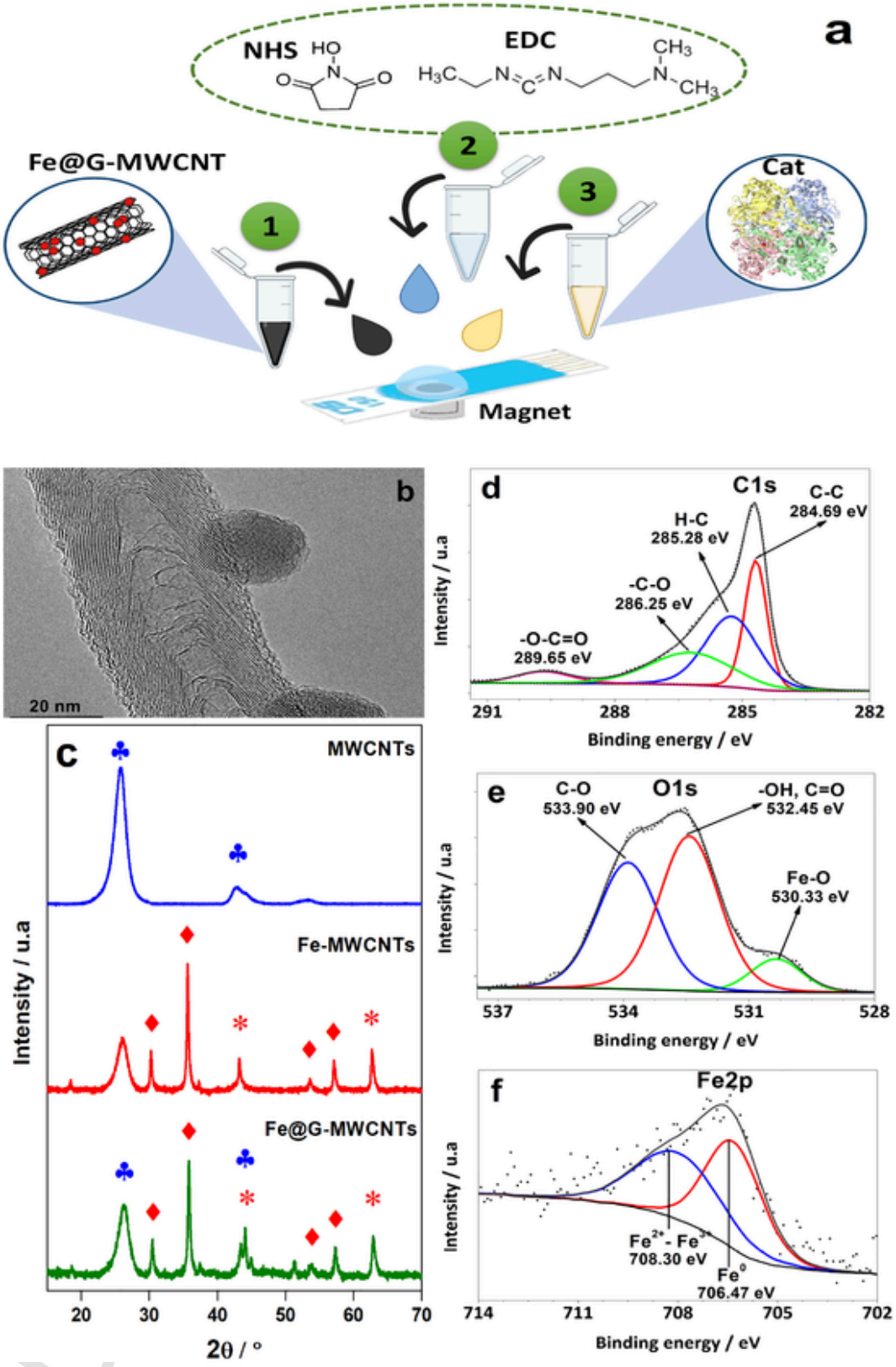

Fig. 1. (a) Schematic diagram of the rational assembly of the enzymatic biosensor. (b) HR-TEM micrograph of Fe@G-MWCNTs. (c) X-ray diffraction pattern of MWCNTs, Fe-MWCNTs and Fe@G-MWCNTs. XPS spectrum for Fe@G-MWCNTs (d) C1s, (e) O1s and (f) Fe2p.

3. Results and discussion

3.1. Characterization of the hybrid nanomaterial

Fig. 1b shows an HR-TEM image of the Fe@G-MWCNTs, where the different structural elements were coexisting as a hybrid nanomaterial. For example, well-defined spherical iron nanoparticles promoting the methane decomposition allowed the deposition of about one to three graphene sheets covering the nanoparticles. Such coating, having a rough surface, could promote the anchorage of a high number of Cat molecules at the hybrid, as demonstrated later. S.I. Fig. S1a shows TEM micrographs at different amplifications, where a random nanotubular network of MWCNTs is supporting some iron nanoparticles of 14 ± 5 nm average size, which nucleation process started preferentially over the defects of the MWCNTs surface [24]. As mentioned in the experimental section, we have employed the microwave-assisted polyol method for impregnating highly monodisperse iron nanoparticles on the MWCNTs surface [25], which resulted in smaller nanoparticles when compared with our previous report [23]. We speculate that having smaller nanoparticles in the hybrid promotes the higher surface area and enhanced electrochemical properties. Furthermore, fewer graphene layers covering the iron nanoparticles isolate them from the medium, protecting them from corrosion, but facilitating the charge transfer through the metal-graphene interface.

TGA measurements gave information on the hybrid nanomaterial's thermal oxidation, which residue at the end of the thermal degradation is essentially iron oxide (Fe_2O_3). Fig. S1b shows TGA curves for Fe@G-MWCNTs, which revealed a low onset degradation temperature around 287 °C, due to incorporating functional groups by oxidative treatment with HNO_3: H_2SO_4 that reduced the initial degradation temperature [26]. The three intermediate peaks at 677, 821, and 861 °C can be attributed to the Fe precursors' decomposition and oxidation of functional groups of the hybrid nanomaterial [24]. The final degradation temperature was around 952 °C, generated by the thermal oxidation of the graphite structures. In general, MWCNTs present thermal oxidation peaks ranging from 500 to 700 °C [26]. However, the incorporation of other materials in the matrix may increase the degradation temperature of the graphitic material [26]. The TGA analysis also revealed a content of 19.7% (in mass fraction) of reduced iron in Fe@G-MWCNTs. X-ray diffraction studies investigated the changes in the crystalline structure of the MWCNTs upon decorating with iron nanoparticles and coating with graphene layers. Fig. 1c shows the X-ray diffraction pattern of the hybrid nanomaterial and its elemental structures. The diffraction peaks at 2θ = 25.8° and 42.7° are attributed to the graphite structure (002) and (100) planes of the MWCNTs [27], while XRD pattern for Fe-MWCNTs nanomaterial shows six characteristic peaks (2θ = 30.4, 35.7, 43.4, 53.6, 57.2, and 62.6°) assigned to the planes: (220), (311), (400), (422), (511), and (440), respectively. The results suggest the presence of iron in a magnetite phase (Fe_3O_4), according to reports in the literature [28,29]. The characteristic peaks of MWCNTs and magnetite remain unchanged after coating with graphene, but it was not possible to differentiate the peaks of MWCNTs and graphene due to the presence of one more graphitic material.

Analysis of the hybrid nanomaterial surface's chemical composition was conducted by X-ray photoelectron spectroscopy (XPS) by studying the binding energy among atoms from their corresponding peaks. XPS spectrums of the hybrid nanomaterials in Fig. 1 d-e show binding energy at 286.25, 289.65, and 532.25 eV, corresponding to C—O, —O—C═O, and O—H/C═O of carboxylic groups. It indicates that carboxylic groups present on the Fe@G-MWCNTs surface are available to be linked to Cat via strong amide bonding. XPS spectrum in Fig. 1f revealed the presence of 65% of Fe^{2+}/Fe^{3+} and 35% Fe^0, in agreement with HR-TEM, TGA, and XRD results. S.I. Fig. S1c shows the XPS spectrum of MWCNTs and Fe-MWCNTs, but no significant differences were observed with respect to the spectrum from Fe@G-MWCNTs.

3.2. Effect of iron content in the electrochemical response of the hybrid nanomaterial

The effect of the iron nanoparticle content on the electrochemical response of the hybrid nanomaterial-modified electrodes was evaluated by CV. S.I. Fig. S2 shows the CV of Fe-MWCNTs and Fe@G-MWCNTs with a nominal iron content of 5 to 20% (in mass fraction) in 1 mM $K_3[Fe(CN)_6]$/PBS 1× (pH 7.2)/N_2 saturated solution. The current intensity ($I_{p,a}$) for the hybrid nanomaterial increased from 13.6 ± 0.2 to 16.4 ± 0.1 μA in an iron content-dependent manner. Besides, peak-to-peak separation (ΔEp) decreased from 131.3 ± 1.3 to 113.0 ± 0.2 mV for 5Fe@G-MWCNTs to 20Fe@G-MWCNTs, respectively; which indicates differences in the electron transfer on the surface of the modified-electrodes. Besides, the hybrid nanomaterial with bare iron nanoparticles (Fe-MWCNTs) showed an electrochemical response very similar to the one from graphene-coated nanoparticles (Fe@G-MWCNTs), especially at 20% iron content (Fig. S2d). This behavior may be related to the fact that iron nanoparticles' electrical conductivity and graphene layers are in the same order of magnitude. The slightly worst electrochemical response of the hybrid nanomaterial coated with graphene layers at lower iron contents may be associated with graphite formation on top of the nanoparticles. Therefore, 20Fe@G-MWCNTs was select as a hybrid nanomaterial for further immobilization of Cat

3.3. Electrochemical characterization of the Cat-immobilized electrode

Fig. 1a depicts the step-by-step rationale assembling of the enzymatic (bio)sensor at the surface of the SPCE by drop-casting bare-, iron decorated- and graphene-coated iron decorated-MWCNTs, i.e., MWCNTs/SPCE, Fe-MWCNTs/SPCE and Fe@G-MWCNTs/SPCE, respectively; and after functionalization of the hybrid nanomaterial with Cat (Cat/Fe@G-MWCNTs/SPCE). The electrochemical response was evaluated in each step of the (bio)sensor assembly by CV and EIS. Fig. 2a shows changes in the voltammetric profiles in 1 mM $K_3[Fe(CN)_6]$/PBS 1× (pH 7.2)/N_2 saturated solution as the SPCE was modified step-by-step with the nanomaterials. We calculated the electroactive area (A) of the electrodes from the CV by the Randles-Sevcik equation [30] as detailed in S.I. Eq. (1)

The pair of redox peaks observed for each modified-electrode are characteristic of the redox probe. The $I_{p,a}$ increased from 14.5 ± 0.20 (SPCE) to 15.9 ± 0.20 (MWCNTs/SPCE), and 16.5 ± 0.01 μA (Fe-MWCNTs/SPCE) as the SPCE was modified, correlated to the increase of the electrochemical area from 9.45 ± 0.13 to 9.98 ± 0.06, and 10.01 ± 0.01 mm^2 for the corresponding modified electrodes, respectively (Table 1). Otherwise, the current intensity showed no significant differences (16.4 ± 0.10 μA) when the graphene layers coated the iron nanoparticles (Fe@G-MWCNTs/SPCE), indicating similar catalytic properties of iron and graphene-coated iron on the surface of the modified-electrode. However, ΔE_p went to 113.1 ± 0.2 mV (Table 1) for Fe@G-MWCNTs as the SPCE was modified, as explained by a barrier to electron transfer of the quasi-reversible system.

EIS in ferro/ferricyanide redox couple determined differences in the electron transfer capability of the hybrid systems. Whereas a Nyquist plot ($-Z''$ vs. Z') represented the results with a semicircle at high frequencies and a linear response at low frequencies (Fig. 2b), a Randles equivalent circuit model fit the experimental data (Fig. 2b, inset). Where R_{ct} is the charge transfer resistance, R_s is the electrolyte resistance, Z_w is the Warburg diffusion element; and CPE is the constant phase element, used often in modeling the response of non-homogeneous systems and used herein to take into account the topological imperfections of the electrode surface and fit better the experimental data

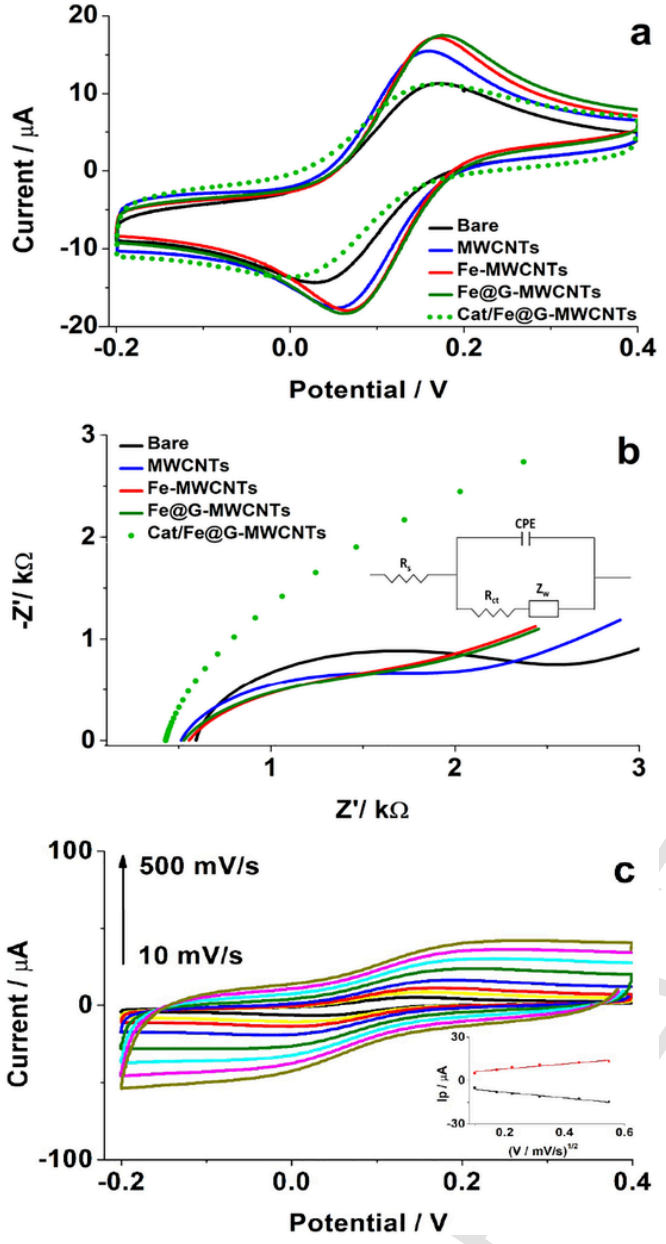

Fig. 2. (a) CV of different modified-electrodes in 1 mM $K_3Fe(CN)_6$/PBS 1× (pH 7.2)/N_2 saturated solution at a scan rate of 50 mV/s for bare SPCE, MWCNTs/SPCE, Fe-MWCNTs/SPCE and Cat/Fe@G-MWCNTs/SPCE. (b) Nyquist plot in 5 mM $[Fe(CN)_6]^{4-/3-}$/PBS 1× (pH 7.2) solution, in the frequency range from 50 kHz to 0.1 Hz, amplitude 0.005 V. (c) CV in 1 mM $K_3Fe(CN)_6/N_2$ saturated PBS 1× (pH 7.2) recorded at the different scan rate of (from inner to outer): 10, 30, 50, 100, 200, 300, 400 and 500 mV/s. Inset, plot of cathodic ($I_{p,c}$) and anodic ($I_{p,a}$) peak current vs the square root of scan rates for Cat/Fe@G-MWCNTs/SPCE.

[18,31,32]. *CPE* depends on a pre-exponential factor (*P*) and an exponent (*n*). *P* values indicated a decrease in the system's capacitive behavior, and *n* values for modified-electrodes were less than one, consistent with a pseudo interfacial double layer capacitance at the electrode/electrolyte interface [23]. The modified-electrode (Fig. 2b) follows a Randles circuit model (shown in Fig. 2b, inset) characteristic of non-homogeneous systems. The R_{ct} decreased from 1799.2 (SPCE) to 1386.4 Ω (Fe-MWCNTs/SPCE) because of a faster charge transfer process. However, after modification with Fe@G-MWCNTs, the R_{ct} was 1409.5 Ω suggesting that graphene layers slightly blocked the redox probe flow and hindered its diffusion towards the modified-electrode surface. However, the R_{ct} further increased up to 3920.8 Ω after the immobilization of Cat onto Fe@G-MWCNTs/SPCE, coming from blocking generated by enzyme molecules on the hybrid-electrode surface [33]. All EIS parameters are summarized in Table 1. Fig. S3 a–b shows comparative CV and EIS spectrums before and after Cat immobilization. These results suggest that the immobilization of Cat increased the capacitive current and the charge transfer resistance on modified-electrodes but indicates that the immobilization of Cat on the modified-electrode was successful.

CV of the different bare hybrid nanomaterials in a 1 mM $K_3[Fe(CN)_6]$/PBS 1× (pH 7.2)/N_2 saturated solution at different scan rate gave us a better insight into the electrochemical process, e.g., the quasi-reversibility of the process involving free diffusing redox species and to estimate the heterogeneous electron-transfer kinetics. $I_{p,a}$ increased as the scan rates did, with a linear dependence of peak current with the square root of the scan rate, consistent with a diffusion-controlled redox process (Fig. 2c and inset for Cat/Fe@G-MWCNTs/SPCE and Fig. S4 for all nanomaterials). Thus, we used the empirical method proposed by Nicholson [34] to estimate the heterogeneous rate constant, k_s, using the dimensionless charge-transfer parameter, Ψ that is associated with the ΔE_p and is proportional to k_s (see S.I. Eqs. (2) and (3)).

K_s raised a maximum value of 6.61 × 10^{-3} cm/s for the Fe-MWCNTs/SPCE and slightly decreased to 5.09 × 10^{-3} cm/s (Table 1) when the graphene layers were coating the Fe nanoparticles from the Fe@G-MWCNTs nanomaterial, consistent with the diffusion limitation of the electrochemical probe through the graphene layers. The K_s value after Cat immobilization is approximately five orders of magnitude lower (1.06 × 10^{-3} cm/s) for Cat/Fe@G-MWCNTs/SPCE compared to the hybrid nanomaterial, indicating much slower electron transfer kinetics of the free-diffusing species, hindered by the Cat molecules on the modified-electrode surface.

3.4. Direct electron transference of Cat

Direct electron transfer between the active center of the redox protein and the electrode surface in enzymatic sensors is desirable to operate without mediators' need. The protein matrix protects the heme group, thus difficulting the electron transfer to the modified-electrode surface [22]. Fig. 3a shows the CV of Cat immobilized on the different modified electrodes in PBS 1× (pH 7.2)/N_2 saturated solution at a scan rate of 0.05 V/s. The Cat/SPCE showed no electrochemical redox peaks in the potential range studied (Fig. 3a, *I*). The reduction of oxygen groups from the nanomaterial surface explained a broad redox peak above - 0.5 V for MWCNTs and Fe-MWCNTs modified-Cat (*II* and *III*) [35]. The Cat/Fe@G-MWCNTs/SPCE showed electrochemical redox peaks in the same potential range studied (Fig. 3a, *IV*). Cat/Fe@G-MWCNTs/SPCE ~~exhibits~~ a well-defined cathodic peak of higher intensity, at a formal potential of - 0.44 V and an anodic peak of lower intensity, at −0.23 V (Fig. 3b), due to conformational changes of Cat during the catalytic process [36]. The redox peak corresponds to the heme group -Fe(III)/Fe(II) redox couple- from catalase [37], coming from the direct electron transfer between Cat and the modified-electrode surface. The unique properties of Fe@G-MWCNTs (e.g., the enhanced electrical conductivity, higher surface area, and MWCNTs-biomolecule strong bonding) explain the facile electron-transfer communication of Cat [38]. S.I. Fig. S5 shows the comparative electrochemical response for direct communication in modified-electrodes, where Cat/Fe@G-MWCNTs/SPCE presented a peak corresponding to the reduction of the heme group from Cat. The inset of Fig. 3b shows the CVs of the Cat/Fe@G-MWCNTs/SPCE electrode in PBS 1× (pH 7.2)/N_2 saturated solution in which the cathodic peak currents are increasing linearly with the scan rate, consistent with a surface-controlled redox process. The entire scan rate study of Cat immobilized on the modified-electrodes is in S.I. Fig. S6. As the density of electroactive redox protein in the surface (Γ_c) follows the Faraday law (S.I. Eq. (4)), we estimated it

Table 1
Electrochemical characterization of the modified-electrodes. Data from cyclic voltammetry experiments in 1 mM $K_3Fe(CN)_6$/PBS 1× (pH 7.2)/N_2 saturated solution at a scan rate of 50 mV/s (left side): Peak anodic current intensity ($I_{p,a}$), anodic and cathodic peak separation (ΔEp), electroactive area (A) and heterogeneous electron-transfer rate constant (k_s). Data from EIS experiments (center): Charge-transfer resistance (R_{ct}), electrolytic solution resistance (R_s), Warburg diffusion element (Z_w), constant phase element (CPE) with pre-exponential factor (P) and exponent (n). Data from cyclic voltammetry experiments PBS 1× (pH 7.2)/N_2 saturated solution at a scan rate of 50 mV/s (right side): surface concentration of electroactive species (Γ_c).

Data from cyclic voltammetry experiments					Equivalent circuit elements from the EIS experiments					Data from direct communication experiments
Electrode Type	$I_{p,a}$ (μA)	ΔE_p (mV)	A (mm^2)	k_s (cm/s) x 10^{-3}	R_{ct} (Ω)	R_s (Ω)	Z_w (Ω)	CPE		Γ_c (mol/cm^2) x 10^{-10}
								P (F)	n	
SPCE	14.5 ± 0.20	98.7 ± 10.9	9.45 ± 0.13	4.94	1799.2	594.1	990.1	1.9×10^{-5}	0.92	–
MWCNTs	15.9 ± 0.20	108.3 ± 5.2	9.98 ± 0.06	5.03	1468.3	513.1	980.3	3.4×10^{-5}	0.82	–
Fe-MWCNTs	16.5 ± 0.01	104.9 ± 3.0	10.01 ± 0.01	6.61	1386.4	556.4	891.2	1.1×10^{-4}	0.75	–
Fe@G-MWCNTs	16.4 ± 0.11	113.0 ± 0.2	9.97 ± 0.11	5.09	1409.5	527.1	872.4	1.0×10^{-4}	0.74	–
Cat/SPCE	8.6 ± 0.20	140.0 ± 4.2	5.27 ± 0.19	1.71	2938.4	401.4	1881.1	3.7×10^{-5}	0.87	0.35
Cat/MWCNTs	10.3 ± 0.01	137.4 ± 0.5	6.20 ± 0.43	1.90	2130.6	535.1	1786.6	5.4×10^{-5}	0.82	0.22
Cat/Fe-MWCNTs	7.5 ± 0.01	158.1 ± 0.2	5.13 ± 0.01	1.55	3725.1	393.4	1791.9	9.8×10^{-5}	0.82	2.96
Cat/Fe@G-MWCNTs	9.05 ± 0.23	171.3 ± 1.1	5.38 ± 0.16	1.06	3920.8	429.5	2188.0	1.9×10^{-4}	0.91	4.41

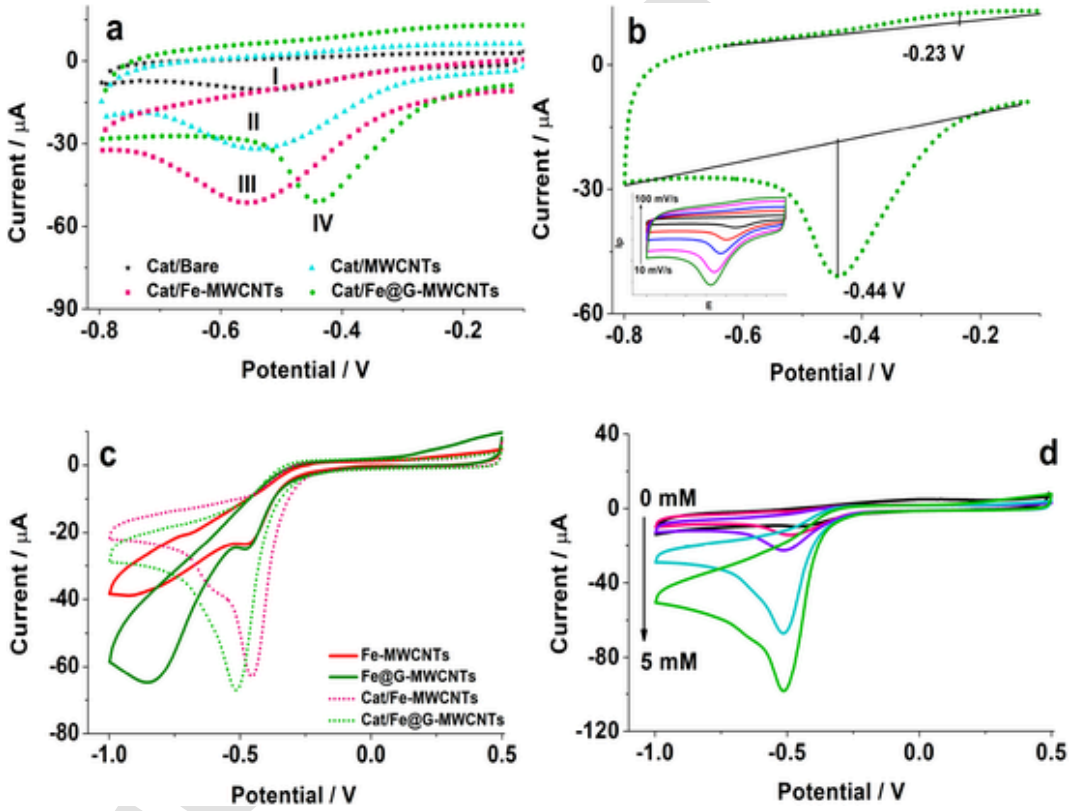

Fig. 3. CV of modified-electrodes in PBS 1× (pH 7.2)/N_2 saturated solution of (a) catalase immobilized on modified-electrodes at scan rate of 50 mV/s: (Curve I) for bare SPCE, (Curve II) MWCNTs/SPCE, (Curve III) Fe-MWCNTs/SPCE, (Curve IV) Fe@G-MWCNTs/SPCE; (b) Cat/Fe@G-MWCNTs/SPCE at scan rate of 50 mV/s. Inset: Cat/Fe@G-MWCNTs/SPCE recorded at the different scan rate of (from inner to outer): 10, 30, 50, 80 and 100 mV/s. CVs of modified-electrodes at a scan rate of 10 mV/s: (c) Comparative response for Cat/Fe-MWCNTs/SPCE, Cat/Fe@G-MWCNTs/SPCE and the same hybrid nanomaterials but without enzyme in 3.0 mM H_2O_2/PBS 1× (pH 7.2)/N_2 saturated solution; (d) Cat/Fe@G-MWCNTs/SPCE in PBS 1× (pH 7.2) solution containing (from inner to outer) 0.0, 0.5, 1.0, 3.0, and 5.0 mM of H_2O_2.

from the slope of peak currents vs. the scan rate plot (data no-showed) [39].

Table 1 displays the calculated surface density of Cat active species at the nanomaterial-modified electrodes, i.e., 0.35×10^{-10} and 0.22×10^{-10} mol/cm^2 for the Cat/SPCE and Cat/MWCNTs modified-electrodes, respectively. The rate of electrons transfers to and from the heme group is susceptible to distance and conformation changes. Therefore, Cat species' activity on the modified-electrode surfaces is due to immobilized Cat molecules in the first few layers that, closer to the electrode surface and having an appropriate orientation, exchange electrons with the electrode surface [33]. The active species of Cat at Cat/Fe-MWCNTs and Cat/Fe@G-MWCNTs modified-electrodes were estimated to be 2.96×10^{-10} and 4.41×10^{-10} mol/cm^2, respectively, in agreement with approximately a monolayer of Cat, as reported [40].

The amount of active catalase is higher on Cat/Fe@G-MWCNTs/SPCE, suggesting that the hybrid nanostructure provides a larger area for the enzyme immobilization [36].

3.5. Electrocatalytic behavior of Cat-modified electrodes towards H_2O_2

The biocatalytic activity of the Cat-modified electrodes towards H_2O_2 was elucidated by CV in the potential range from 0.5 to −1.0 V at 0.01 mV/s scan rate. Fig. 3c shows the typical CV of the hybrid nanomaterial-modified electrodes with and without Cat in the presence of 3.0 mM of H_2O_2. The catalytic reduction of H_2O_2 showed to be an irreversible process. The Cat-functionalized hybrid nanomaterial led to a higher current intensity of the H_2O_2 reduction peak with respect to the concomitant bare hybrid nanomaterial counterparts. Such a response is a probe of the enhanced catalytic activity from the anchored enzyme, which was previously reported in the literature [40] (see the catalytic mechanism in the S.I. section).

The Cat catalytic mechanism depends on pH. S.I. Fig. S7 shows the effect of pH on the electrochemical response of the Cat immobilized on the modified electrodes. According to Fig. S7 at pH's above or below 7.2, a lower electrochemical response is observed in the decomposition of H_2O_2. The highest activity for the Cat immobilized on the modified electrode was obtained in PBS 1× (pH 7.2)/N_2 saturated solution, which is close to the optimal pH of free Cat [41].

Furthermore, the reduction peak at the Cat/Fe-MWCNTs/SPCE surface at −0.45 V shifted towards a more cathodic potential at the Cat/Fe@G-MWCNTs/SPCE surface (− 0.50 V), indicating a slight overpotential needed for the electron-transfer process [35]. Fig. 3d shows that the cathodic peak's current intensity at the Cat/Fe@G-MWCNTs/SPCE is increasing in an H_2O_2 concentration-dependent manner. Both the cathodic peak current increase and the potential decrease indicate the electrocatalysis phenomena [42]. The enzymatic catalysis from Cat immobilized at the hybrid nanomaterial nano-environment, combined with the hybrid's ability to mediate electrocatalytic processes, resulted in the improved response of the Cat/Fe@G-MWCNTs/SPCE platform towards H_2O_2 depletion.

3.6. Amperometry determination of H_2O_2 at the modified electrode

The amperometric response of the Cat/Fe-MWCNTs and Cat/Fe@G-MWCNTs upon different H_2O_2 concentrations were evaluated in PBS 1× (pH 7.2)/N_2 saturated solution at a fixed potential of −0.65 V. Fig. 4 a-b shows current intensity increased with increasing concentrations of H_2O_2, with the insets showing the linear dependence. The resultant Cat/Fe-MWCNTs/SPCE (bio)sensor showed a high electrocatalytic activity towards the reduction of H_2O_2 with a linear response from 0.5 to 12 mM, a sensitivity of 0.047 μA/(μM.cm^2), and a LOD of 165.2 μM. The Cat/Fe@G-MWCNTs/SPCE (bio)sensor responded from 0.1 to 7 mM, with enhanced sensitivity of 0.059 μA/(μM.cm^2) and a lower LOD of 28.2 μM. LOD was determined by the $3\sigma_b/m$ criteria. Although the two (bio)-sensors analytical performance is comparable, the LOD achieved with the Cat/Fe@G-MWCNTs/SPCE is almost 6-fold lower than that from the Cat/Fe-MWCNTs/SPCE, in agreement with their estimated differences in Cat surface coverage. The results indicate that the hybrid nanomaterial provides both a high surface area and a suitable microenvironment for the Cat immobilization. Indeed, the mild conditions in terms of temperature and pH, the short time and the simple preparation used in developing the (bio)sensor agree with some other reports [19,21]. These conditions favor conserving the Cat's activity during its immobilization at the hybrid nanomaterial modified-electrode. The LOD of the developed (bio)sensors were higher than those previously reported by chronoamperometry [22,43,44]. Yet, the developed (bio)sensors showed higher sensitivity than some other reports [19,45,46].

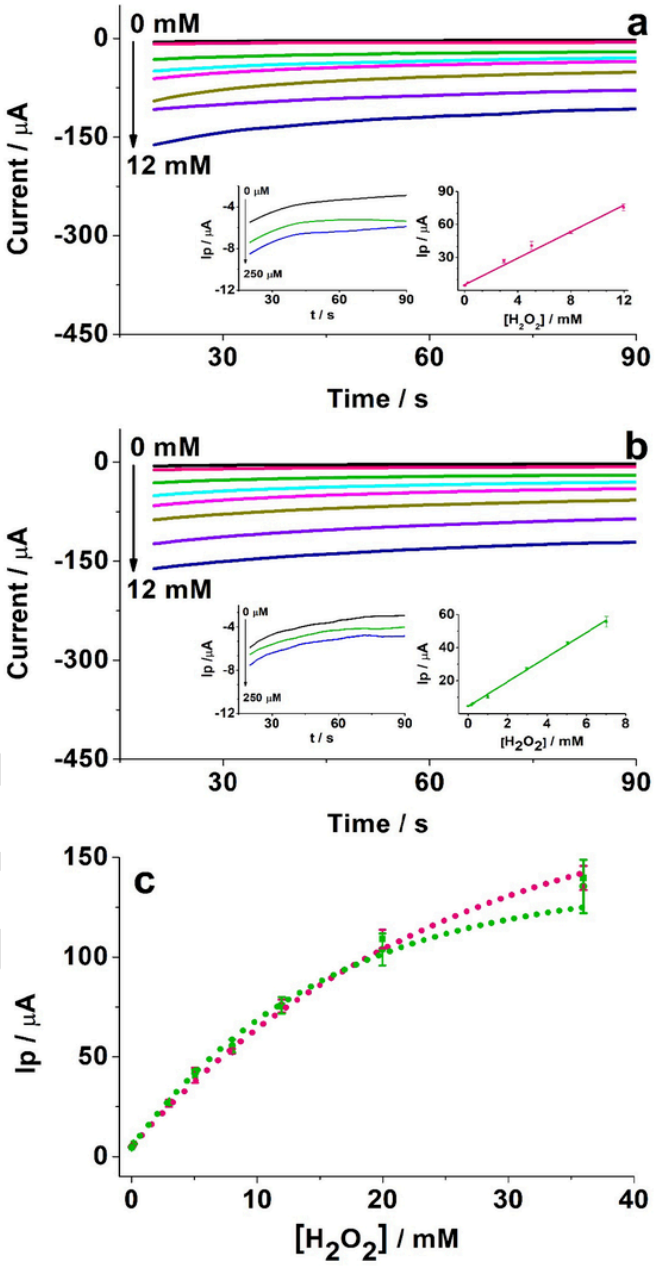

Fig. 4. Amperometric response at (a) Cat/Fe-MWCNTs/SPCE, (b) Cat/Fe@G-MWCNTs/SPCE and (c) Michaelis–Menten plot. Addition of [illegible] 2.0 mM of H_2O_2 at an applied potential of −0.65 V in a PBS 1× (pH 7.2) [illegible]saturated solution. The insets are plots of current intensity response vs. [H_2O_2] from [illegible] 250 μM (left) and the corresponding calibration curve (right).

Cat immobilized at the surface of the hybrid nanomaterials displayed a catalytic current depending on the concentration of H_2O_2 that follows the Michaelis–Menten kinetic mechanism (Fig. 4c). To study the enzyme kinetics at both electrodes and to evaluate the Cat-substrate affinity, we estimated the Michaelis–Menten constant ($K^{app}{}_M$) from the Lineweaver–Burk equation (S.I. see Eq. (5)) [47].

The $K^{app}{}_M$ and I_{max} were 19.5 mM and 199.2 μA, and 17.9 mM and 191.2 μA for the Cat/Fe-MWCNTs/SPCE and Cat/Fe@G-MWCNTs/SPCE. Remarkably, the $K^{app}{}_M$ values were lower than those reported for the free Cat, i.e. 43.42 mM [48]. Although the $K^{app}{}_M$ of catalase commonly increases after covalent immobilization [48], in this study, the $K^{app}{}_M$ values for Cat/Fe-MWCNTs/SPCE and Cat/Fe@G-MWCNTs/SPCE decreased by 2.2 and 2.4-fold, with respect to the free-enzyme respec-

tively, indicating a higher Cat-substrate affinity. The I_{max} and the enzyme-substrate affinity of Cat immobilized at the Fe@G-MWCNTs/SPCE were slightly higher than those at the Fe-MWCNTs/SPCE, which is related to higher active species of Cat on the hybrid-electrode. The overall results suggest the enhanced performance of the enzyme supported at the hybrid nanomaterial interfaces, which impacted the resultant (bio)sensors' improved electrochemical characteristics in terms of sensitivity and LOD. Such improved performance may be coming from an improved conformation of the enzyme that lower both the steric hindrance to access the active sites and the resistance to mass and charge transport [49] at the hybrid nanomaterial-anchored enzyme.

3.7. Storage stability, reproducibility and repeatability studies

Long-term stability is one of the most important properties for (bio)sensors. We studied the long-term stability of the Cat-modified hybrid nanomaterial-modified SPCEs by monitoring their response every five days for twenty-five days based on the 3σ criteria (Fig. 5a). The (bio)sensors were stored in PBS 1× (pH 7.2) at 4 °C and the stability was estimated by potting a control chart taking the mean value of the amperometry responses from five successive measurements and considering the first day of the study as the initial value. The upper and lower control limits were set at three times the standard deviation (3σ) of this value. Results showed that after 25 days of storage, only the Cat/Fe@G-MWCNTs/SPCE was in between the control limits and retained 95.4% of its initial response, while the Cat/Fe-MWCNTs/SPCE retained only 87.0%, being out of the control limits. The developed (bio)sensor showed higher storage stability with respect to other reported sensor platforms [21,22]. The stability of the (bio)sensors is related to the nanomaterials' high stability and the high Cat-hybrid structure affinity. Moreover, these results demonstrate the protective effect of graphene layers on iron nanoparticles' catalytic activity by delaying their oxidation processes, thereby increasing the long-term stability of the hybrid architecture. Although the long-term stability was studied for one month due to the deterioration of the SPCE contacts, we speculate that the Cat-modified hybrid nanomaterial stability maybe longer. Five Cat/Fe@G-MWCNTs/SPCEs were prepared independently and their electrocatalytic responses measured towards a 3.0 mM H_2O_2 solution, five times each, under identical experimental conditions (Fig. 5b) to investigate the repeatability and reproducibility of the (bio)sensors response. The intra- and inter-electrode relative standard deviation (RSD) was estimated to be 3.50 (n = 5) and 6.75% (n = 5), which indicates the high repeatability and reproducibility of the (bio)sensors developed, respectively.

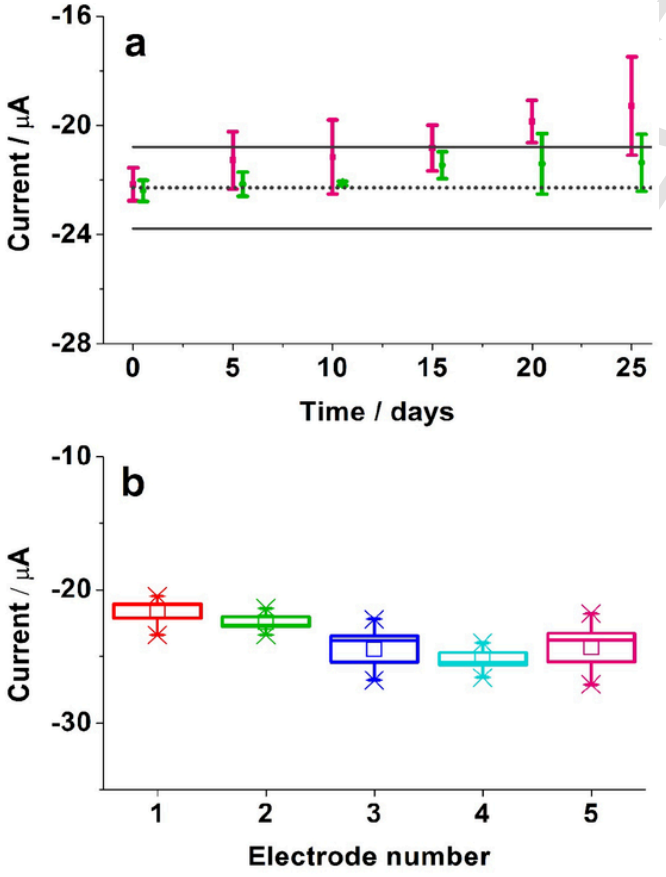

Fig. 5. (a) Long-term stability of catalase immobilized on the hybrid nanomaterial-modified electrode for one month. (b) Reproducibility and repeatability studies of Cat/Fe@G-MWCNTs. Operational conditions: Chronoamperometry response at applied potential of −0.65 V in 3.0 mM H_2O_2/PBS 1× (pH 7.2)/N_2 saturated solution.

3.8. Analytical application

The practical applicability of the Cat/Fe@G-MWCNTs/SPCE (bio)sensors was probed by testing the H_2O_2 concentration in commercially available samples by chronoamperometry and compared to nominal values (Table 2). The H_2O_2 concentration was calculated by extrapolating the current values obtained for each commercial sample in the calibration curve depicted in Fig. 4b. After considering the dilution factor, the concentration of H_2O_2 in the commercial sample determined by Chronoamperometry showed a relative error lower than 5.2% with respect to the reported concentration for each commercial sample (Table 2). Furthermore, an ANOVA test suggests no significant differences for the 4 and 3.6% H2O2 contained in antiseptic solution and Dioxogen samples, respectively, compared with the nominal values for each commercial sample ($p > 0.05$). However, for creamy lotion of 9.0% H_2O_2 content, there are significant differences ($p < 0.05$) associated with the sample matrix's complexity. H_2O_2 levels from the hybrid nanomaterial-based (bio)sensor correlated well with those reported by the manufacturer of the commercially available products, thus demonstrating the device's practical utility.

4. Conclusion

It was developed a new Cat-functionalized hybrid nanomaterial based on MWCNTs decorated with iron nanoparticles, covered with graphene layers, and systematically compared their electrochemical performance. The results showed the enhanced properties of the hybrid platform concerning the individual components acting alone. The hybrid showed a suitable microenvironment for Cat's direct electrochemistry and maintained its bioactivity and stability. Cat/Fe@G-MWCNTs/SPCE exhibited biocompatibility, a higher amount of immobilized-active species and improved Cat redox activity. Such improved features impacted the enhanced electrochemical performance of the resultant (bio)sensor towards H2O2 in terms of sensitivity and LOD and long-term stability and high reproducibility. Although this is the first proof-of-concept of the hybrid nanomaterial as an enzymatic (bio)sensor, it

Table 2
Hydrogen peroxide measurements in commercial samples using the Cat/Fe@G-MWCNTs/SPCE biosensor.

Commercial sample	$[H_2O_2]$ (mM)		Relative error (%)
	Manufacturer	Biosensor	
Antiseptic JgB® (4.0%)	3.79	3.64 ± 0.15	3.9
Dioxogen JgB® (3.6%)	3.85	3.94 ± 0.14	2.3
Creamy lotion (9.0%)	3.70	3.51 ± 0.03	5.2

offers potential as a platform to develop hybrid nanomaterial-based (bio)sensors in a myriad of applications in the environmental and biomedical fields.

Uncited reference

[3]

CRediT authorship contribution statement

Dayana Soto: Conceptualization, Methodology, Validation, Formal analysis, Investigation, Writing - original draft, Visualization. **Manuela Alzate:** Investigation. **Jaime Gallego:** Resources, Writing - review & editing. **Jahir Orozco:** Conceptualization, Formal analysis, Resources, Writing - review & editing, Supervision, Project administration.

Declaration of Competing Interest

None.

Acknowledgments

J.O and D.S thank the financial support provided by COLCIENCIAS, University of Antioquia and the Max Planck Society through the Cooperation agreement 566-1, 2014. J. G. acknowledges COLCIENCIAS and the University of Antioquia for the support of the project 1115-715-51427.

Appendix A. Supplementary data

Supplementary data to this article can be found online at https://doi.org/10.1016/j.jelechem.2020.114826.

References

[1] M. Carraro, S. Gross, Hybrid materials based on the embedding of organically modified transition metal oxoclusters or polyoxometalates into polymers for functional applications: a review, Materials (Basel). 7 (2014) 3956–3989, doi:10.3390/ma7053956.
[2] Y.L. Xie, S.Q. Zhao, H.L. Ye, J. Yuan, P. Song, S.Q. Hu, Graphene/CeO2 hybrid materials for the simultaneous electrochemical detection of cadmium(II), lead(II), copper(II), and mercury(II), J. Electroanal. Chem. 757 (2015) 235–242, doi:10.1016/j.jelechem.2015.09.043.
[3] S. Mondal, D. Khastgir, Elastomer reinforcement by graphene nanoplatelets and synergistic improvements of electrical and mechanical properties of composites by hybrid nano fillers of graphene-carbon black & graphene-MWCNT, Compos. Part A Appl. Sci. Manuf. 102 (2017) 154–165.
[4] F.A. Gutierrez, M.D. Rubianes, G.A. Rivas, New bioanalytical platform based on the use of avidin for the successful exfoliation of multi-walled carbon nanotubes and the robust anchoring of biomolecules. Application for hydrogen peroxide biosensing, Anal. Chim. Acta 1065 (2019) 12–20, doi:10.1016/j.aca.2019.03.022.
[5] G.A. Rivas, M.C. Rodríguez, M.D. Rubianes, F.A. Gutierrez, M. Eguílaz, P.R. Dalmasso, E.N. Primo, C. Tettamanti, M.L. Ramírez, A. Montemerlo, P. Gallay, C. Parrado, Carbon nanotubes-based electrochemical (bio)sensors for biomarkers, Appl. Mater. Today 9 (2017) 566–588, doi:10.1016/J.APMT.2017.10.005.
[6] T. Feng, Y. Wang, X. Qiao, Recent advances of carbon nanotubes-based electrochemical immunosensors for the detection of protein cancer biomarkers, Electroanalysis. 29 (2017) 662–675, doi:10.1002/elan.201600512.
[7] P. Dhanjai, A. Balla, L. Sinha, X. Wu, D. Lu, J. Tan, Chen, Co3O4 nanoparticles supported mesoporous carbon framework interface for glucose biosensing, Talanta. 203 (2019) 112–121, doi:10.1016/j.talanta.2019.05.056.
[8] G. Maduraiveeran, W. Jin, Functional nanomaterial-derived electrochemical sensor and biosensor platforms for biomedical applications, Handb. Nanomater. Anal. Chem. (2020) 297–327, doi:10.1016/B978-0-12-816699-4.00012-8.
[9] C. Tyagi, N. Chauhan, A. Tripathi, U. Jain, D.K. Avasthi, Voltammetric measurements of neurotransmitter-acetylcholine through metallic nanoparticles embedded 2-D material, Int. J. Biol. Macromol. 140 (2019) 415–422, doi:10.1016/j.ijbiomac.2019.08.102.
[10] S. Panhwar, S.S. Hassan, R.B. Mahar, K. Carlson, M. Ul, H. Rajput, M.Y. Talpur, Highly Sensitive and selective electrochemical sensor for detection of *Escherichia coli* by using L-cysteine functionalized iron nanoparticles, J. Electrochem. Soc. 166 (2019) 30179–30185, doi:10.1149/2.0691904jes.
[11] W. Zhang, C. Wang, L. Guan, M. Peng, K. Li, Y. Lin, A non-enzymatic electrochemical biosensor based on Au@PBA(Ni–Fe):MoS2 nanocubes for stable and sensitive detection of hydrogen peroxide released from living cells, J. Mater. Chem. B 7 (2019) 7704–7712, doi:10.1039/C9TB02059D.
[12] D. Alzate, S. Cajigas, S. Robledo, C. Muskus, J. Orozco, Genosensors for differential detection of Zika virus, Talanta. 210 (2020) 120648, doi:10.1016/j.talanta.2019.120648.
[13] Z.J. Zhang, Z.L. Wang, B.C. Chakoumakos, J.S. Yin, Temperature dependence of cation distribution and oxidation state in magnetic Mn–Fe ferrite nanocrystals, J. Am. Chem. Soc. 120 (1998) 1800–1804, doi:10.1021/JA973085L.
[14] Y. Li, Y. Hu, G. Huang, C. Li, Metallic iron nanoparticles: flame synthesis, characterization and magnetic properties, Particuology. 11 (2013) 460–467, doi:10.1016/J.PARTIC.2012.10.008.
[15] R. Malik, V.K. Tomer, V. Chaudhary, Hybridized Graphene for Chemical Sensing, in: Funct, Elsevier, Graphene Nanocomposites Their Deriv, 2019, pp. 323–338, doi:10.1016/B978-0-12-814548-7.00016-7.
[16] D. Prasai, J.C. Tuberquia, R.R. Harl, G.K. Jennings, K.I. Bolotin, Graphene: corrosion-inhibiting coating, ACS Nano 6 (2012) 1102–1108, doi:10.1021/nn203507y.
[17] S. Ren, M. Cui, W. Li, J. Pu, Q. Xue, L. Wang, N-doping of graphene: toward long-term corrosion protection of cu, J. Mater. Chem. A 6 (2018) 24136–24148, doi:10.1039/c8ta05421e.
[18] S. Singal, A.K. Srivastava, S. Dhakate, A.M. Biradar, R. Rajesh, Electroactive graphene-multi-walled carbon nanotube hybrid supported impedimetric immunosensor for the detection of human cardiac troponin-I, RSC Adv. 5 (2015) 74994–75003, doi:10.1039/C5RA15449A.
[19] A.T.E. Vilian, S.-M. Chen, B.-S. Lou, A simple strategy for the immobilization of catalase on multi-walled carbon nanotube/poly(l-lysine) biocomposite for the detection of H2O2 and iodate, Biosens. Bioelectron. 61 (2014) 639–647, doi:10.1016/J.BIOS.2014.05.023.
[20] Y.G. Mourzina, A. Offenhäusser, Electrochemical properties and biomimetic activity of water-soluble meso-substituted Mn(III) porphyrin complexes in the electrocatalytic reduction of hydrogen peroxide, J. Electroanal. Chem. 866 (2020) 114159, doi:10.1016/j.jelechem.2020.114159.
[21] P. Rahimi, H.A. Rafiee-Pour, H. Ghourchian, P. Norouzi, M.R. Ganjali, Ionic-liquid/NH2-MWCNTs as a highly sensitive nano-composite for catalase direct electrochemistry, Biosens. Bioelectron. 25 (2010) 1301–1306, doi:10.1016/j.bios.2009.10.020.
[22] A.P. Periasamy, Y.H. Ho, S.M. Chen, Multiwalled carbon nanotubes dispersed in carminic acid for the development of catalase based biosensor for selective amperometric determination of H2O2 and iodate, Biosens. Bioelectron. 29 (2011) 151–158, doi:10.1016/j.bios.2011.08.010.
[23] D. Soto, M. Alzate, J. Gallego, J. Orozco, Electroanalysis of an Iron@Graphene-carbon nanotube hybrid material, Electroanalysis. 30 (2018) 1521–1528, doi:10.1002/elan.201800115.
[24] J. Gallego, J. Tapia, M. Vargas, A. Santamaria, J. Orozco, D. Lopez, Synthesis of graphene-coated carbon nanotubes-supported metal nanoparticles as multifunctional hybrid materials, Carbon N. Y. 111 (2017) 393–401, doi:10.1016/j.carbon.2016.10.014.
[25] B.K. Park, S. Jeong, D. Kim, J. Moon, S. Lim, J.S. Kim, Synthesis and size control of monodisperse copper nanoparticles by polyol method, J. Colloid Interface Sci. 311 (2007) 417–424, doi:10.1016/j.jcis.2007.03.039.
[26] E.R. Edwards, E.F. Antunes, E.C. Botelho, M.R. Baldan, E.J. Corat, Evaluation of residual iron in carbon nanotubes purified by acid treatments, Appl. Surf. Sci. 258 (2011) 641–648, doi:10.1016/j.apsusc.2011.07.032.
[27] X.J. Fan, X. Li, Preparation and magnetic properties of multiwalled carbon nanotubes decorated by Fe3O4 nanoparticles, New Carbon Mater. 27 (2012) 111–116, doi:10.1016/S1872-5805(12)60007-9.
[28] D. Sivkov, O. Petrova, A. Mingaleva, A. Ob'edkov, B. Kaverin, S. Gusev, I. Vilkov, S. Isaenko, D. Bogachuk, R. Skandakov, V. Sivkov, S. Nekipelov, The structure and chemical composition of the Cr and Fe pyrolytic coatings on the MWCNTs' surface according to NEXAFS and XPS spectroscopy, Nanomaterials. 10 (2020) 1–22, doi:10.3390/nano10020374.
[29] L. Wang, H. Qiu, C. Liang, P. Song, Y. Han, Y. Han, J. Gu, J. Kong, D. Pan, Z. Guo, Electromagnetic interference shielding MWCNT-Fe3O4@Ag/epoxy nanocomposites with satisfactory thermal conductivity and high thermal stability, Carbon N. Y. 141 (2019) 506–514, doi:10.1016/j.carbon.2018.10.003.
[30] L. Jiang, J. Han, F. Li, J. Gao, Y. Li, Y. Dong, Q. Wei, A sandwich-type electrochemical immunosensor based on multiple signal amplification for α-fetoprotein labeled by platinum hybrid multiwalled carbon nanotubes adhered copper oxide, Electrochim. Acta 160 (2015) 7–14, doi:10.1016/J.ELECTACTA.2015.02.050.
[31] X. Dominguez-Benetton, S. Sevda, K. Vanbroekhoven, D. Pant, The accurate use of impedance analysis for the study of microbial electrochemical systems, Chem. Soc. Rev. 41 (2012) 7228–7246, doi:10.1039/c2cs35026b.
[32] B. Kumar, V. Bhalla, R.P. Singh Bhadoriya, C.R. Suri, G.C. Varshney, Label-free electrochemical detection of malaria-infected red blood cells, RSC Adv. 6 (2016) 75862–75869, doi:10.1039/C6RA07665C.
[33] F. Liu, Q. Xu, W. Huang, Z. Zhang, G. Xiang, C. Zhang, C. Liang, H. Lian, J. Peng, Green synthesis of porous graphene and its application for sensitive detection of hydrogen peroxide and 2,4-dichlorophenoxyacetic acid, Electrochim. Acta 295 (2019) 615–623, doi:10.1016/j.electacta.2018.10.177.
[34] R.S. Nicholson, Theory and application of cyclic voltammetry for measurement of electrode reaction kinetics, Anal. Chem. 37 (1965) 1351–1355, doi:10.1021/ac60230a016.
[35] H.L. Guo, X.F. Wang, Q.Y. Qian, F. Bin Wang, X.H. Xia, A green approach to the synthesis of graphene nanosheets, ACS Nano 3 (2009) 2653–2659, doi:10.1021/nn900227d.
[36] B. Kowalewska, K. Jakubow, The impact of immobilization process on the electrochemical performance, bioactivity and conformation of glucose oxidase enzyme, Sensors Actuators B Chem. 238 (2017) 852–861, doi:10.1016/j.snb.2016.07.138.
[37] S.W. Ting, A.P. Periasamy, S.M. Chen, R. Saraswathi, Direct electrochemistry of catalase immobilized at electrochemically reduced graphene oxide modified electrode for amperometric H2O2 biosensor, Int. J. Electrochem. Sci. 6 (2011) 4438–4453.

[38] Z. Zhu, An overview of carbon nanotubes and graphene for biosensing applications, Nano-Micro Lett. 9 (2017) 1–24, doi:10.1007/s40820-017-0128-6.
[39] J. Wang, Study of Adsorption Processes, in: Anal, Electrochem, Second, VCH, 1999, p. 38.
[40] G. Fusco, P. Bollella, F. Mazzei, G. Favero, R. Antiochia, C. Tortolini, Catalase-based modified graphite electrode for hydrogen peroxide detection in different beverages, J. Anal. Methods Chem. 2016 (2016) 1–13, doi:10.1155/2016/8174913.
[41] M. Bartoszek, W. Sułkowski, The study of pH influence on bovine liver catalase by means of UV-VIS spectroscopy and spin labelling method, Pol. J. Environ. Stud. 15 (2006) 41–43.
[42] E.S. Rountree, B.D. Mccarthy, T.T. Eisenhart, J.L. Dempsey, Evaluation of homogeneous electrocatalysts by cyclic voltammetry, Inorg. Chem. 53 (2014) 9983–10002, doi:10.1021/ic500658x.
[43] B. Unnikrishnan, Y.-L. Yang, S.-M. Chen, Amperometric determination of folic acid at multi-walled carbon nanotube-polyvinyl sulfonic acid composite film modified glassy carbon electrode, Int. J. Electrochem. Sci. 6 (2011) 3224–3237.
[44] M. Shamsipur, M. Asgari, M.G. Maragheh, A.A. Moosavi-Movahedi, A novel impedimetric nanobiosensor for low level determination of hydrogen peroxide based on biocatalysis of catalase, Bioelectrochemistry. 83 (2012) 31–37, doi:10.1016/j.bioelechem.2011.08.003.
[45] H.J. Jiang, H. Yang, D.L. Akins, Direct electrochemistry and electrocatalysis of catalase immobilized on a SWNT-nanocomposite film, J. Electroanal. Chem. 623 (2008) 181–186, doi:10.1016/j.jelechem.2008.07.024.
[46] A. Salimi, A. Noorbakhsh, M. Ghadermarzi, Amperometric detection of nitrite, iodate and periodate at glassy carbon electrode modified with catalase and multi-wall carbon nanotubes, Sensors Actuators B Chem. 123 (2007) 530–537, doi:10.1016/j.snb.2006.09.054.
[47] R.A. Kamin, G.S. Wilson, Rotating ring-disk enzyme electrode for biocatalysis kinetic studies and characterization of the immobilized enzyme layer, Anal. Chem. 52 (1980) 1198–1205, doi:10.1021/ac50058a010.
[48] H. Wu, C. Zhang, Y. Liang, J. Shi, X. Wang, Z. Jiang, Catechol modification and covalent immobilization of catalase on titania submicrospheres, J. Mol. Catal. B Enzym. 92 (2013) 44–50, doi:10.1016/j.molcatb.2013.03.018.
[49] S.S. Tukel, O. Alptekin, Immobilization and kinetics of catalase onto magnesium silicate, Process Biochem. 39 (2004) 2149–2155, doi:10.1016/J.PROCBIO.2003.11.010.